ISSN 1990-3413, Astrophysical Bulletin, 2018, Vol. 73, No. 3, pp. 267–278. © Pleiades Publishing, Ltd., 2018.
Original Russian Text © F.G. Kopylova, A.I. Kopylov, 2018, published in Astrofizicheskii Byulleten', 2018, Vol. 73, No. 3, pp. 281–293.

Outskirts of Galaxy Clusters A 1139, A 1314, A 1656, A 2040, A 2052, A 2107: Star-Formation Rate

F. G. Kopylova* **and A. I. Kopylov**

Special Astrophysical Observatory, Russian Academy of Sciences, Nizhnii Arkhyz, 369167 Russia

Received December 19, 2017; in final form, June 6, 2018

Abstract—We investigate the variation of the fraction of galaxies with suppressed star formation ($M_K < -21\overset{\mathrm{m}}{.}5$) and early-type galaxies ($frac_E$) of the "red sequence" along the projected radius in six galaxy clusters: Coma (A 1656), A 1139, and A 1314 in the Leo supercluster region ($z \approx 0.037$) and A 2040, A 2052, A 2107 in the Hercules supercluster region ($z \approx 0.036$). According to SDSS (DR10) data, $frac_E$ is the highest in the central regions of galaxy clusters and it is, on the average, equal to 0.62 ± 0.03, whereas in the $2{-}3R/R_{200c}$ interval and beyond the $R_{sp} \approx 0.95 \pm 0.04\ R_{200m}$ radius that we inferred from the observed profile $frac_E$ is minimal and equal to 0.25 ± 0.02. This value coincides with the estimate $frac_E = 0.24 \pm 0.01$ that we inferred for field galaxies located between the Hercules and Leo superclusters at the same redshifts. We show that the fraction of galaxies with suppressed star formation decreases continuously with cluster radius from 0.87 ± 0.02 in central regions down to 0.43 ± 0.03 in the $2{-}3\ R/R_{200c}$ interval and beyond R_{sp}, but remains, on the average, higher than 26% than the corresponding fraction for field objects. This decrease is especially conspicuous in the galaxy mass interval $\log M_* [M_\odot] = 9.5{-}10$. We found that galaxies with ongoing star formation have average clustercentric distances $1.5{-}2.5\ R/R_{200c}$ and that their radial-velocity dispersions are higher than those of galaxies with suppressed star formation.

DOI: 10.1134/S199034131803001X

Key words: *galaxies: clusters—galaxies: evolution—galaxies: star formation*

1. INTRODUCTION

Galaxy clusters are dynamic objects, which grow by accreting galaxies and groups of galaxies along filaments from the surrounding space. As a result of their continuous growth galaxy clusters harbor the virialized component, which consists mostly of old early-type galaxies and the population of galaxies recently accreted from outside. In the dense inner medium of clusters galaxies acquire properties that differ from those of field galaxies—star formation becomes suppressed in cluster galaxies. Various physical mechanisms are acting in this medium, which result in the decrease of the gas content in galaxies and ultimately in the decrease of star-formation rate. These mechanisms include tidal interactions between galaxies or between galaxies and the potential well of the cluster; galaxy harassment, ram pressure stripping, and thermal evaporation (see review [1] for details). Note that the decrease of the star-formation rate in rich galaxy clusters is observed in galaxies of all types unlike what we see in field galaxies [2]. The slowdown of star-formation rate is also observed along the cluster radius towards the center (for the galaxy cluster sample with $0.19 < z < 0.55$ [3], x-ray bright galaxy clusters with $0.15 < z < 0.30$ [4], and catalog of groups of galaxies from SDSS DR7 [5]). Based on the results of observations of 30 massive galaxy clusters ($0.15 < z < 0.30$) Haines et al. [4] found that the fraction of star-forming cluster galaxies is lower than among the field population even at the clustercentric distance of $3R_{200}$. The above authors conclude that this phenomenon can be explained by assuming that star-forming galaxies must go through the virialized region of the cluster over 0.5–2.0 Gyr before leaving it.

N-body simulations [3] of the star-formation gradient along the galaxy cluster radius showed that a significant fraction of galaxies beyond the virial radius of the cluster (out to $2R_{vir}$) have spent some time in their central regions. Studies of galaxy properties at cluster peripheries based on N-body simulations [6] also showed that the fraction of such ("splashback") galaxies between $1{-}2\ R_{vir}$ is of about 50%. Such galaxies have twice lower velocities compared to the galaxies that have entered the virialized part of the cluster for the first time. When crossing the virialized part of the cluster "splashback" galaxies lose about 40% of their mass. However, simulations of the

*E-mail: flera@sao.ru

x-ray emitting region of the inner medium in galaxy clusters [7] showed that spiral galaxies lose their gas before entering the virialized region and this process naturally results un the decrease of the star-formation rate in these objects.

When investigating star-formation rate in nearby clusters ($0.04 < z < 0.07$) Paccagnella et al. [8] found a population of galaxies (which rarely occur in the field) intermediate between star-forming galaxies and quiet galaxies without star formation.

The position of the galaxy in the phase-space diagram is commonly used to better understand the role that the immediate surroundings of the galaxy play in its evolution. The projected phase-space diagram of galaxy clusters reflects the dependence of the projected distance of the galaxy from the chosen center on its normalized radial velocity. This diagram can be used to investigate, e.g., the star-formation gradient in clusters and how it is related to the position of galaxies on the diagram, as well as to the fact that certain galaxies belong to the "old" population of the cluster, or have just fallen onto the cluster, or have left the virialized region (splashback galaxies) (see, e.g., [9–14]).

The aim of this study is (1) to determine the dynamical properties of the nearby galaxy clusters A 1139 and A 1314 (in the Leo supercluster region), A 2052, A 2107, and A 2040 (in the Hercules supercluster region), A 1656, and their peripheral regions described by different radii and (2) to investigate the variation of the specific star formation rate ($sSFR$) and the fraction of galaxies exhibiting no star formation along normalized radius and as a function of stellar mass.

This study uses the data of the SDSS (Sloan Digital Sky Survey Data Release 10 [15]) and 2MASS XSC (Two-Micron ALL-Sky Survey Extended Source Catalog [16]) catalogs and NED (NASA Extragalactic Database).

The paper has the following layout. The second section describes the procedure of the measurement of dynamical properties of galaxies and determination of the cluster outskirt. In the third section we construct the color-magnitude sequence for early-type galaxies in galaxy systems and determine the fraction of early-type galaxies. The fourth section gives the distributions of the specific star formation rate of galaxy clusters computing assuming fixed stellar mass in galaxies and without such assumption. We demonstrate the gradient of star-formation rate along the normalized radius of galaxy systems computed assuming fixed stellar mass of galaxies and without such assumption, and compare these estimates with the star-formation rate in the field. The concluding section summarizes the main results.

Throughout this study we adopted the following values of cosmological parameters: $\Omega_m = 0.3, \Omega_\Lambda = 0.7$, $H_0 = 70\ \mathrm{km\,s^{-1}\,Mpc^{-1}}$.

2. DYNAMICAL PROPERTIES OF GALAXIES

The completeness of the sample of galaxy systems investigated in this study is determined by the completeness of the spectroscopic data of the SDSS catalog. If the conditions $r_{\mathrm{Pet}} < 17\overset{\mathrm{m}}{.}77$ and $\langle\mu_r\rangle < 24\overset{\mathrm{m}}{.}5/\square''$ (r-band Petrosyan magnitude of the galaxy an the average Petrosyan surface brightness corrected for foreground Galactic extinction corresponding to the effective radius) are satisfied then the completeness of SDSS data is estimated at 99% [17] (95% for bright galaxies).

To increase the spectroscopic completeness of bright galaxies, we used the radial-velocity measurements of bright galaxies (from 1 to 10 for different galaxy systems) for which such measurements are lacking in the SDSS. If no such measurements could be found in the NED database, we selected bright early-type galaxies of the "red sequence" (RS) [18] as likely cluster members (1 to 5 galaxies) based on their positions on the color-magnitude diagrams ($u-r, r$; $g-r, r$; $r-i, r$) [19].

We measured the dynamical properties of galaxy systems—radial velocity, radial-velocity dispersion, and mass for the region of radius $R_{200\mathrm{c}}$. The $R_{200\mathrm{c}}$ radius is the radius of the sphere inside which the density in the system is 200 times higher than the critical density of the Universe, and this radius can be estimated by the formula $R_{200\mathrm{c}} = \sqrt{3}\sigma/10H(z)$ Mpc [20]. The $R_{200\mathrm{m}}$ radius (which is often used in model computations) is equal to the radius of the sphere inside which the density of the system is 200 times higher than the average density of the Universe. We then assume that the cluster is virialized inside this radius $M_{200} \sim M_{\mathrm{vir}}$, to determine the mass $M_{200} = 3G^{-1}R_{200\mathrm{c}}\sigma^2_{200}$. Thus the cluster mass that we measure in this study $M_{200} \propto \sigma^3$. The mass M_{200} contained within the spherical halo of radius $R_{200\mathrm{c}}$ can be estimated directly from the critical density, which depends on z: $M_{200} = \dfrac{4}{3}\pi R^3_{200\mathrm{c}}\,200\rho_c$. In the adopted cosmological model the system must also be virialized for the greater radius $R_{100ë} \approx 1.3R_{200\mathrm{c}}$ [21].

The relations between the mass M_{200} of galaxy systems determined from the dispersion of radial velocities and the K-band luminosity, as well as the mass-luminosity relation and other parameters (based on SDSS DR7 data) for the clusters studied can be found in our earlier papers [22–24].

To characterize in more detail the structure and kinematics of A 2040 (by way of example) and also

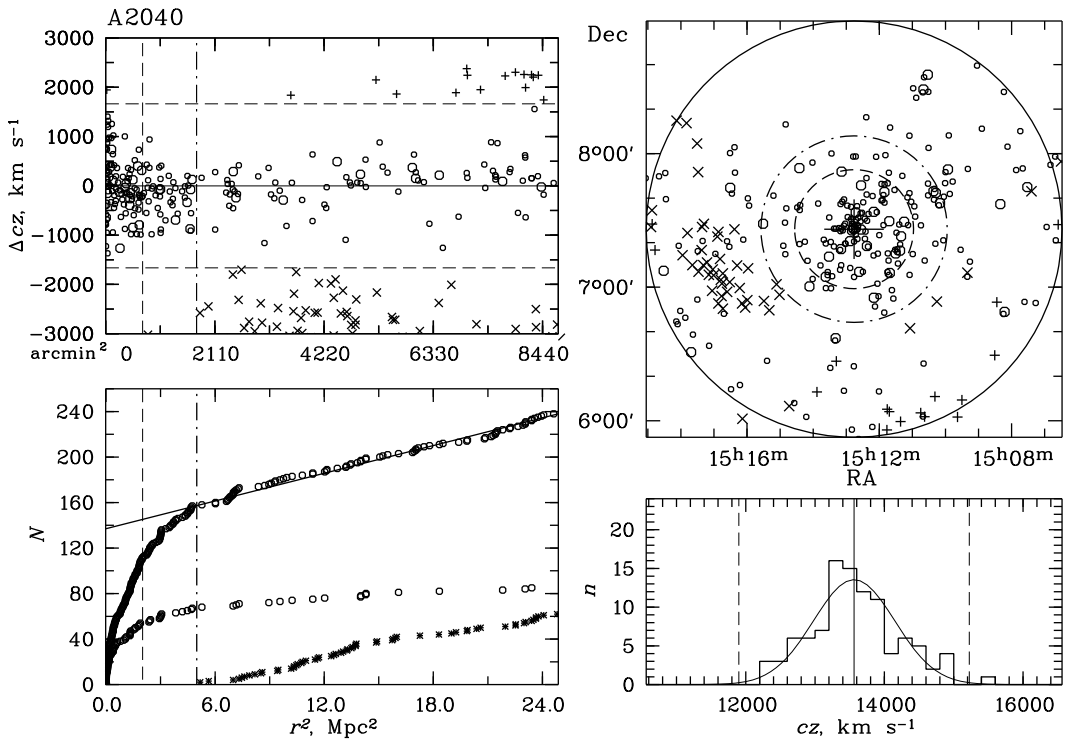

Fig. 1. Distribution of galaxies in the A 2040 cluster. The top left panel shows the deviation of radial velocities of galaxies from the mean radial velocity of the cluster determined from galaxies located within the R_{200c} radius. The horizontal dashed lines correspond to $\pm 2.7\sigma$ deviations and the vertical dashed line indicates the R_{200c} radius. The larger circles indicate galaxies brighter than $M_K^* + 1 = -24^{\rm m}$; the pluses, the background galaxies, and the crosses, the foreground galaxies. The bottom left panel shows the integrated distribution of the total number of galaxies (the upper curve) as a function of the squared distance from the center of the group. The lower curve shows the distribution of early-type galaxies brighter than $M_K < -21\overset{\rm m}{.}5$. The circles show the distribution of galaxies designated by circles in the top left figure, the crosses show the distribution of field galaxies. The dashed-and-dotted line indicates the "splashback" radius $R_{\rm sp}$. The top right panel shows the sky distribution (in equatorial coordinates) of the galaxies presented in the top left panel (same designations are used).The circles outline the region of radius R_{200c} (dashes) and $R_{\rm sp}$ (the dashed-and-dotted circle). The region studied is bounded by the circle of radius $3.5R_{200c}$ (the solid line). The large cross indicates the center of the cluster. The bottom right panel shows the distribution of radial velocities of all galaxies located inside the R_{200c} radius (the solid lines shows the Gaussian for cluster members corresponding to the velocity dispersion for the group). The solid vertical line indicates the average radial velocity of the group and the dashed lines correspond to $\pm 2.7\sigma$ deviations.

its immediate neighborhood, we show in Fig. 1: (1) deviations of radial velocities of cluster members and field galaxies from the average radial velocity plotted as a function of the squared clustercentric radius (the top left figure); (2) the integrated distribution of the number of galaxies as a function of the squared radius (the bottom left figure);(3) location of galaxies in the sky plane in equatorial coordinates (the top right figure); (4)the histogram of radial velocities of all galaxies located within the radius R_{200c} (the bottom right figure).

The bottom left figure shows the projected cluster profile (integrated distribution of the number of galaxies as a function of squared clustercentric distance), which shows that initial steep increase of the number of galaxies followed by linear increase (the straight line) of the number of galaxies located outside the virialized region [24]. The dashed line shows the radius of the virialized region R_{200c} and the dashed-and-dotted line shows the radius that we earlier denoted as R_h, beyond which the initial steep increase of the number of cluster members gives way to linear increase. The lower curve in the same figure shows the distribution of early-type galaxies brighter than $M_K = -21\overset{\rm m}{.}5$, which we use to refine the radius in question. Kopylov and Kopylova [24] assumed that it is the radius of the envelope (halo) surrounding the virialized region. However, the term halo is usually employed to denote the dark halo of the cluster and that is why we changed the designation R_h, which

we employed in [24]. Furthermore, a more detailed analysis showed that for massive galaxy clusters like A 1656, A 1795 the point beyond which the distribution becomes linear (the radius R_h) is located at 3–4 R_{200c}, which is twice farther than reported in [24]. We redetermined the R_h radii for massive galaxy clusters. Given that $R_{vir} > R_{200c}$, it can be assumed that our inferred R_h radius is equal to the radius of the virialized cluster region, R_{vir}. We found that the R_h radius for galaxy clusters studied varies from $1.4R_{200c}$ to $1.84R_{200c}$; on the average, it is equal to $1.55R_{200c}$. On the average, the R_h radius is greater than R_{100c} ($R_{100c} \approx 1.3R_{200c}$) by 14%, i.e., the observed radius R_h that we found is most likely equal to the "splashback"-radius R_{sp} of the galaxy system (the apocentric radius of galaxy orbits) reached by galaxies escaping from the virialized region after the first crossing of the cluster center. Thus the radius R_{sp} separates galaxies, which fall onto the cluster for the first time, from collapsing galaxies, which already take part in the establishment of virial equilibrium.

According to N-body simulations [25], this maximum "rebound" reached by galaxies is between 1–2.5 R_{vir}. Dark halo simulations showed that for rapidly accreting halo the cluster radius beyond which the steepness of the halo surface density profile increases abruptly is $R_{sp} = 0.8$–$1.0\,R_{200m}$ [26]. For slowly accreting halos $R_{sp} \sim 1.5R_{200m}$. The radius R_{sp} found for the halo possibly corresponds to R_{sp} for galaxies. The results of observations of groups and clusters of galaxies yielded the following radii: $R_{sp} \approx 1.33R_{200c}$ [27]; the steepness of the profile of the surface density of galaxies in clusters (SDSS DR8 data) begins to increase at the radius $R_{sp} = 1.43$ Mpc [28]; $R_{sp} = 1.66 \pm 0.08$ Mpc [29] for clusters of galaxies (DES Y1 sample). For the six systems studied the radius R_{sp} that we inferred from the integrated distribution of the number of galaxies as a function of the squared clustercentric distance is, on the average, equal to $1.55 \pm 0.06\,R_{200c}$, or $0.95 \pm 0.04\,R_{200m}$ (given that $4R_{200c} \approx 2.5R_{200m}$). This value is greater than the estimate obtained in [27], but it is consistent with the results of simulations (see, e.g., [26]).

The results of the measurements of the properties of galaxy clusters within the region of radius R_{200} for the clusters studied in this paper are summarized in Table 1: (1) the cluster name; (2) radial velocity dispersion with the cosmological correction $(1+z)^{-1}$ applied; (3)the R_{200c} radius in Mpc; (4) and (5)—the R_{200m} and R_{sp} radii in Mpc; (6) the number of galaxies used to determine the redshift and radial velocity dispersion; (7) measured redshift; (8) the mass M_{200c} measured with the error ρ_c corresponding to the σ measurement error.

3. THE COLOR-MAGNITUDE SEQUENCE ("RED SEQUENCE") OF GALAXY CLUSTERS IN THE PHASE SPACE

The population of galaxy clusters at small redshifts $0 < z < 0.1$ consists mostly of early-type galaxies (see, e.g., [30]), which are mostly located in central virialized regions and are the brightest members of the galaxy systems. The main feature of early-type galaxies is the dependence of galaxy color on magnitude (the brighter the galaxy the redder it is), which suggests the existence of the so called "red sequence" (RS) of galaxy clusters with a small scatter—the universal [31] sequencer of shapes and dispersion values spanning at least 8^m (see, e.g., [18]). The properties of the RS also determine its main applications: identification of galaxy clusters and determination of their distances [32]. Early-type galaxies in virialized cluster regions make up for about 60–70% of all galaxies brighter than $M_K = 23\overset{m}{.}3$ (see, e.g., [19]). In this study we use RS galaxies in order to better investigate the peripheral regions of the clusters considered ($R < 3R_{200c}$).

Figure 2 shows the projected phase-space diagrams, where $\Delta V/\sigma$ is the ratio of the difference of galaxy radial velocities and the mean radial velocity of the cluster to the dispersion of radial velocities and R/R_{200c} is the distance of the galaxy from the adopted cluster center normalized to the R_{200c} radius. We adopt the coordinates of the brightest galaxy as the position of the center of the system of galaxies (except for the A 1656 cluster where we computed the centroid of galaxies located within the R_{200c} radius, which turned out to be close to the radiation center of the x-ray region). The vertical lines in the figures indicate the R_{200c} R_{sp} radii. We illustrate in Fig. 1 the selection of the members of a galaxy cluster within 2.7σ by the example of the A 2040, and in these diagrams we show only selected galaxies.

We selected early-type galaxies based on the following criteria (SDSS, r-band images): $fracDeV \geq 0.8$, where $fracDeV$ is name of the galaxy parameter in the catalog, which characterizes the contribution of the bulge to the surface brightness profile of the galaxy; $r_{90}/r_{50} \geq 2.6$, where the concentration index $c = r_{90}/r_{50}$ is equal to the ratio of the radii containing 90% and 50% of the Petrosian flux. We further imposed the color constraint $\Delta(u-r) > -0.2$, which follows from our inferred dependence of the $u-r$ color on the Petrosian magnitude for clusters, e.g., for Her system: $u - r = -0.078\,r_{Pet} + 3.81$ c $2\sigma = -0.2$. Figure 3 shows the red sequences of galaxy clusters based on selected early-type galaxies satisfying the condition $-0.075 < g - r < 0.075$. These galaxies are shown by circles in this figure and in phase-space diagrams.

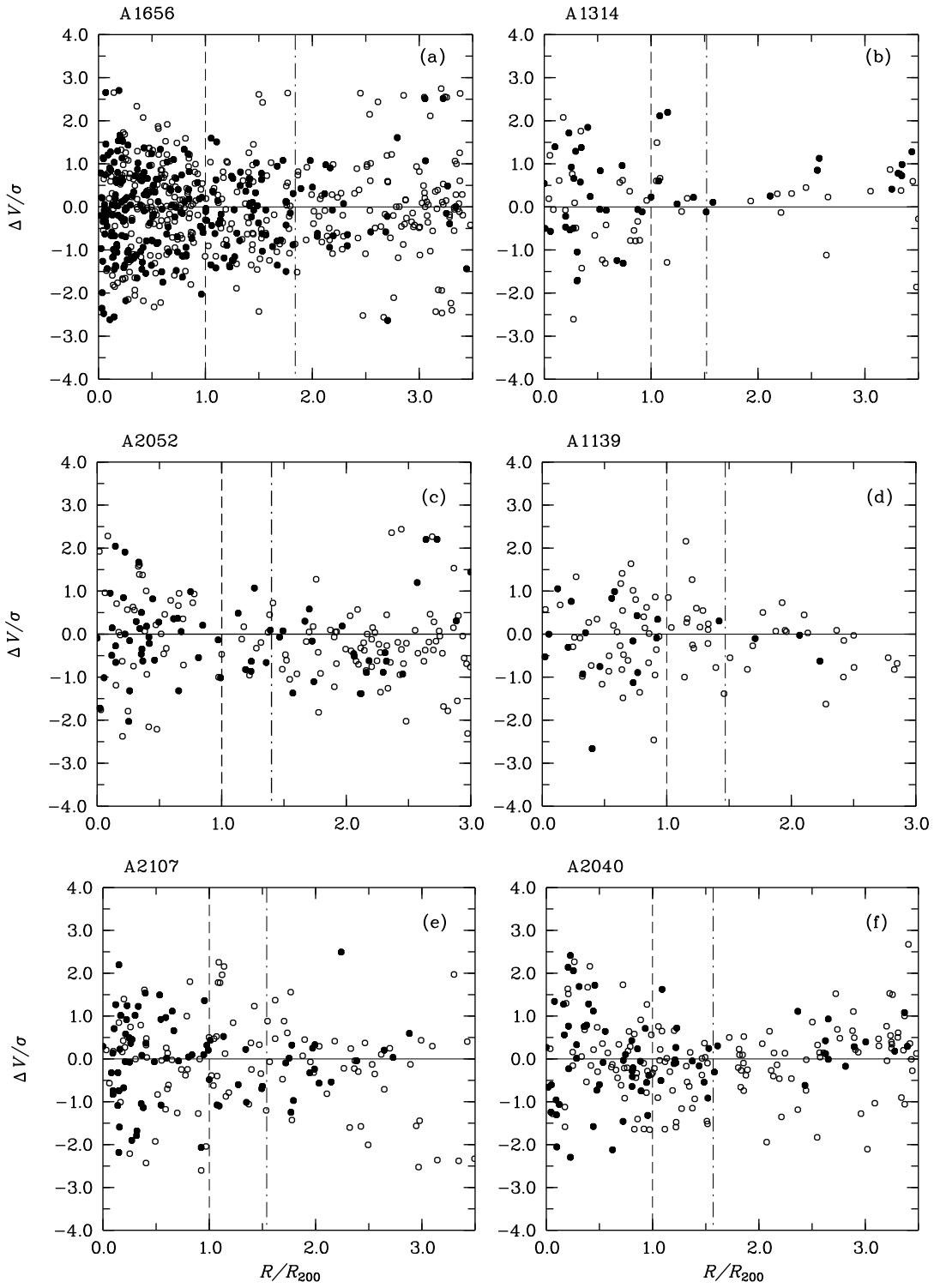

Fig. 2. The velocity vs. radius phase-space diagram for galaxy clusters A 1656, A 1314, A 2052, A 1139, A 2107, and A 2040. Velocity is the ratio of the difference of the radial velocities of galaxies and the average radial velocity of the cluster to the dispersion of radial velocities. The radius R/R_{200c} is equal to the clustercentric distance of the galaxy normalized to the R_{200c} radius. The filled circles show early-type galaxies of the RS. The dashed and dashed-and-dotted lines indicate the R_{200c} and R_{sp} radii, respectively. Galaxies are selected within the 2.7σ limits.

Table 1. Dynamic properties of galaxy clusters

Cluster	σ, km s^{-1}	R_{200c}, Mpc	R_{200m}, Mpc	R_{sp}, Mpc	N_z	z_h	M_{200c}, $10^{14}\ M_\odot$
(1)	(2)	(3)	(4)	(5)	(6)	(7)	(8)
A 1656	921 ± 34	2.255	3.62	4.17	717	0.023250	13.33 ± 1.48
A 1314	492 ± 53	1.182	1.89	1.82	85	0.032443	1.94 ± 0.72
A 2052	623 ± 58	1.517	2.43	2.12	116	0.034726	4.10 ± 1.15
A 1139	459 ± 51	1.115	1.79	1.64	80	0.039327	1.64 ± 0.55
A 2107	581 ± 55	1.411	2.26	2.17	113	0.041335	3.32 ± 0.95
A 2040	589 ± 59	1.427	2.29	2.23	100	0.045242	3.45 ± 1.04

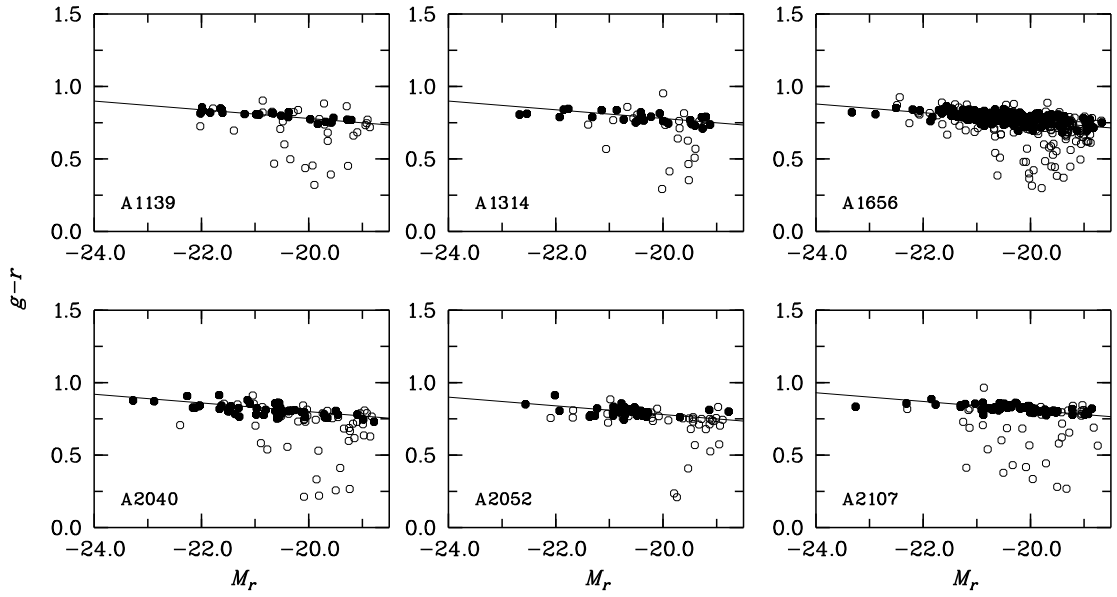

Fig. 3. Color-absolute magnitude diagrams (g–r, M_r). The filled circles show the RS of galaxy clusters.

Note that the bulk of RS galaxies are located in central parts of clusters within our inferred R_{sp} radius. However, at the same time a part of the galaxies are located at the clustercentric distance $3R_{200c}$. We found that the fraction of early-type RS galaxies decreases by a factor of two from 0.51 ± 0.02 within $R < 1R/R_{200c}$ down to 0.25 ± 0.02 within $2R/R_{200c} < R < 3R/R_{200c}$. Beyond the R_{sp} radius (which, on the average, is equal to $1.55 \pm 0.06 R_{200c}$) $frac_E$ is also equal to 0.25 ± 0.03. The results of our study of the variation of the fraction of early-type galaxies along the normalized radius are summarized in Table 2.

To compare the results obtained for galaxy clusters (i.e., dense regions) with those obtained for low-density regions, we selected two regions free of galaxy clusters (practically, field regions), and determined the corresponding fraction of early-type galaxies based on SDSS DR10 data. Our selected cluster-free fields are located between the Hercules and Leo superclusters: the first field is centered at $14^{\rm h}.5$, 35°, has a radius of 300 arcmin and spans the redshift interval $0.030 < z < 0.045$, and the second field is centered at $13^{\rm h}.5$, 5°, has the same size and its objects span a similar redshift interval. We select early-type galaxies in these fields based on the same criteria: $fracDeV \geq 0.8$, $r_{90}/r_{50} \geq 2.6$, $(g-r)$>0.65. We described the measurement of K_s-band luminosities in our earlier papers [22, 23]. The first field contains a total of 219 galaxies with

$M_K < -21\overset{\mathrm{m}}{.}5$ including 49 early-type galaxies, i.e., the fraction of early-type galaxies is 0.22 ± 0.04. We found 147 galaxies including 40 early-type galaxies in the second field, where the corresponding fraction is 0.27 ± 0.05. The fraction of early-type galaxies averaged over the two fields is 0.24 ± 0.01. As we pointed out above, similar fractions—0.25 ± 0.02 and 0.25 ± 0.03—are observed in galaxy clusters within their nearest neighborhood, $2 < R/R_{200c} < 3$ and $R > R_{sp}$ (Table 2). The fraction of early-type galaxies within the $1 < R/R_{200c} < 2$ clustercentric distance interval is higher than in the field and equal to 0.36 ± 0.05. We thus showed that most of the early-type galaxies of the cluster is contained within the radius $R < R_{sp}$ determined from observations: some of them are already virialized and some (according to simulations performed by Rhee et al. [14]) have escaped from the virialized region and will again return to it after reaching the orbital apocenter R_{sp} inferred here.

4. SPECIFIC STAR-FORMATION RATE IN GALAXY CLUSTERS

The first determinations of the star-formation rate in galaxies were published in [33, 34]. The specific star-formation rate ($sSFR$) in a galaxy is defined as the integrated star-formation rate divided by the stellar mass, $sSFR = SFR/M_*$. The SDSS catalog (DR10) gives the inferred stellar masses of galaxies and their specific star-formation rates determined by fitting FSPS models [35]. The fits are based on extinction-corrected SDSS u, g, r, i, and z-band model magnitudes and "early-star formation with dust" version.

The galaxy clusters studied here have masses spanning the $\log M_{200c}[M_\odot] = 14.21$–$15.12$ interval. Figure 4 shows the $sSFR$ distributions for all galaxies (Fig. 4p) and separately for galaxies with stellar mass in the intervals (in $M_\odot$): $\log M_\star =$ 9.5–10.0, 10.0–10.5, 10.5–11.0, and 11.0–11.5. The distribution has a long tail on the left side. The distribution for each cluster is shown by an individual line. The distribution usually has a minimum separating galaxies with ongoing star formation (active galaxies) from galaxies with suppressed star formation (quenched galaxies). Conspicuous bimodality of the distribution and the minimum corresponding to $\log sSFR[\mathrm{yr}^{-1}] = -11$ were found, e.g., in [5], where $sSFR$ was determined from Hα emission and discontinuity at 4000 Å. As is evident from Fig. 1 in the above paper, in the halo mass interval $\log M_{halo}[M_\odot] = 14.3$–$15.0$ (as in the case of the galaxy clusters that we investigate in this study) the minimum in the distribution is poorly defined, although the peak is quite conspicuous. In our case it is evident from Fig. 4a that the minimum in the distributions for three galaxy clusters studied (A 1314, A 1656, and A 2107) corresponds to $\log sSFR[\mathrm{Gyr}^{-1}] \approx -1.5$, or $\log sSFR[\mathrm{yr}^{-1}] \approx -10.5$, whereas the distributions for the three remaining systems have minima at lower values, and we therefore adopted for all system the common minimum equal to $\log sSFR[\mathrm{Gyr}^{-1}] = -1.75$. The $\log sSFR[\mathrm{Gyr}^{-1}] \sim -2.2$ corresponds to the maximum. Wetzel et al. [5] determined that for SDSS DR7 galaxy systems the fraction of quenched galaxies increases with stellar mass of galaxies. We show the dependence of the $sSFR$ distribution on stellar mass of the galaxy $\log M_\star$ in Fig. 4b–4e. Note that star formation in galaxies with stellar masses $\log M_\star = 11.0$–11.5 (Fig. 4d) is suppressed, like is the case in the stellar mass interval $\log M_\star = 10.5$–11.0. In the stellar mass interval $\log M_\star = 9.5$–10.0 the fraction of galaxies with suppressed star formation exceeds the fraction of "active" galaxies only in the clusters A 1656 and A 1139, whereas other clusters contain a significant fraction of "active" galaxies.

Density in galaxy clusters decreases withe distance from the adopted center, and the location of a galaxy at a certain radius is related to the time when it arrived in the cluster (see, e.g., [4]). Fig. 5 shows the fractions of quenched galaxies as a function of projected cluster radius normalized by R_{200c}. Galaxy clusters are binned according to the M_{200c} mass: A 2040, A 2052 and A 2107, A 1139 and A 1314, and the richest cluster A 1656 is considered individually. Fig. 5a shows the total fraction of galaxies with suppressed star formation in the clusters considered for all stellar masses, and Figs. 5b–5e show this galaxy fraction for each stellar-mass interval separately. The total fraction of galaxies with suppressed star formation from the mean value of 0.87 ± 0.02 within 0–$0.25\ R/R_{200c}$ to 0.43 ± 0.03 within 2–$3\ R/R_{200c}$. Thus the fraction of galaxies with suppressed star formation decreases to $3R/R_{200c}$ by 51%. The most significant variations of the fraction of quenched galaxies can be seen in Fig. 5b for low-mass galaxies with stellar masses $\log M_\star[M_\odot] = 9.5$–$10.0$, except for the A 1656, which a system with a mass of $M_{200c}[M_\odot] > 10^{15}$. Star formation is suppressed practically in all galaxies with stellar masses $\log M_\star[M_\odot] = 10.5$–$11.5$ (Fig. 5d and, especially, Fig. 5e). The last bin contains too few galaxies and therefore the curves are poorly outlined. Note that some of the galaxies in central regions (4% in A 1656 and 2% in other clusters) having spectral information in SDSS DR10 lack star-formation rate measurements. We found the mean fraction of galaxies with suppressed star formation (averaged over two fields)

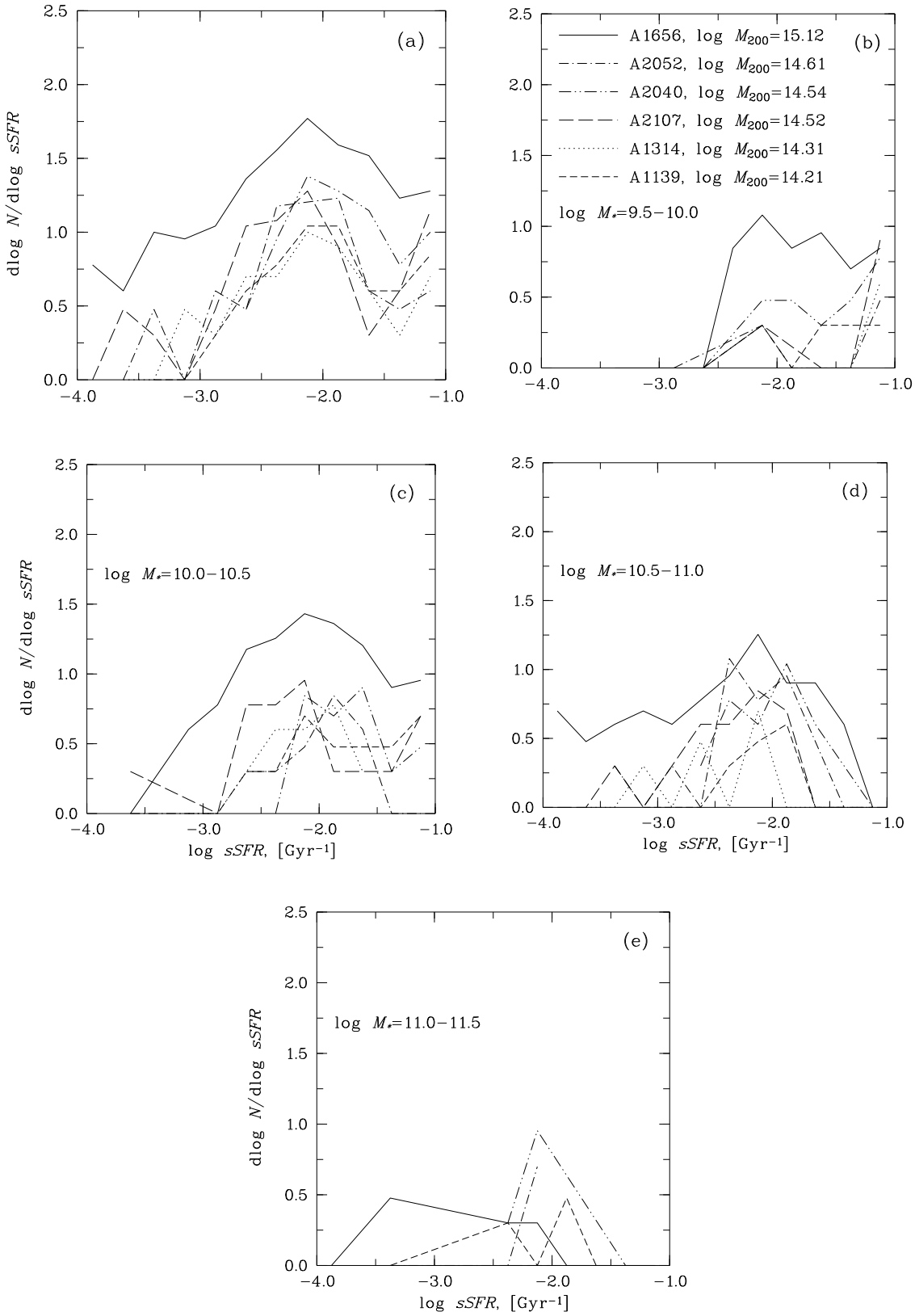

Fig. 4. Distribution of specific star-formation rates ($sSFR$) of galaxies: (a) for all galaxy clusters; (b), (c), (d), and (e) for subsamples of galaxies binned by stellar masses. The masses M_{200c} and $M_\star$ are in $M_\odot$.

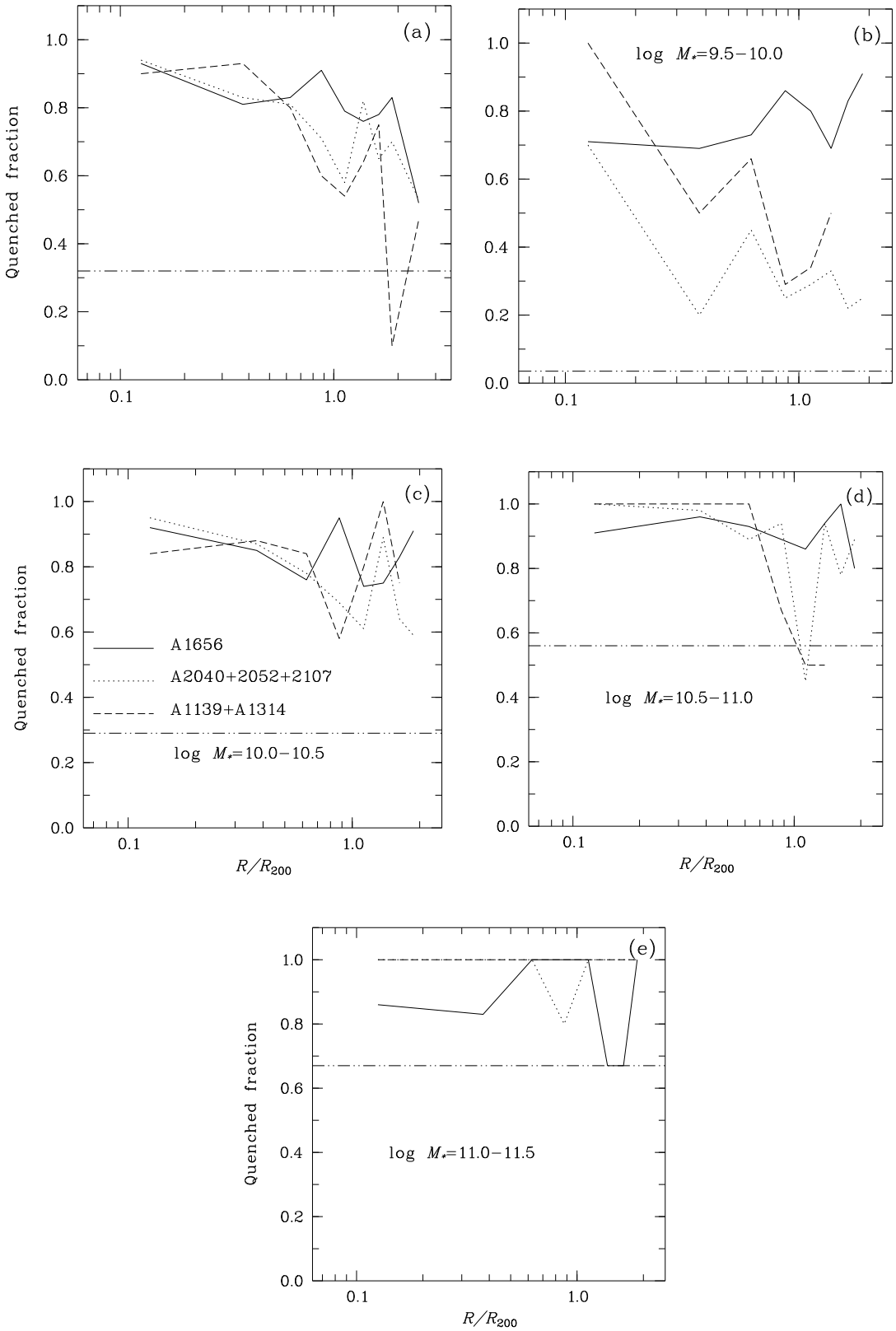

Fig. 5. Fraction of galaxies with suppressed star formation ($\log sSFR[\mathrm{Gyr}^{-1}] < -1.75$) as a function of projected cluster-centric distance. Clusters are grouped by mass. Panel (a) shows the fraction for all clusters, and panels (b), (c), (d), and (e)—the corresponding fractions for subsamples of galaxies of these clusters binned by stellar mass. The dashed-and-dotted line in each figure shows the fraction of quenched field galaxies. Masses M_{200} and $M_\star$ are in $M_\odot$.

satisfying the condition $\log sSFR[\mathrm{Gyr}^{-1}] < -1.75$. It is equal to 0.32 ± 0.07, which is less by 63% than in central regions of galaxy clusters and less by 55% than within the R_{sp} radius, or less by 26% than within $2{-}3\ R/R_{200\mathrm{c}}$.

Haines et al. [4] show for 30 galaxy clusters with $0.15 < z < 0.30$ that even within the $3R_{200\mathrm{c}}$ the fraction of galaxies with ongoing star formation is lower and hence the fraction of galaxies with suppressed star formation is higher than in the field. Wetzel et al. [36] established, based on SDSS R7 data, that excess of galaxies with suppressed star formation is observed outside the virial radius of the system of galaxies (down to $2.5R_{\mathrm{vir}}$). Thus even outside virialized regions of galaxy clusters the fraction of quenched galaxies remains higher than in the field. Spirals, which are not classified as early-type galaxies, also contain a fraction of galaxies with suppressed star formation. We determined this fraction among spiral galaxies by parameters $du - r < -0.2$, $deVfr < 0.8$ and $r_{90}/r_{50} < 2.6$. As expected, central regions of galaxy clusters ($0{-}0.25\ R/R_{200\mathrm{c}}$) contain no spiral quenched galaxies, the fraction of these objects is maximal outside the virialized region within $1{-}2\ R/R_{200\mathrm{c}}$, where it amounts, on the average, to 0.11 ± 0.02 (except the clusters A 1139 and A 1314). In the clustercentric interval $2{-}3\ R/R_{200\mathrm{c}}$ spiral quenched galaxies with a mean fraction of 0.14 ± 0.06 can be found only in the A 1656, A 2107, and A 2052 clusters. In dense environments in galaxy clusters spiral galaxies with suppressed star formation are found and their fraction is higher than in the field [37]. The dashed-and -dotted curves in Fig. 5 show the fractions of quenched galaxies in the field for each interval of stellar masses. Note that the fraction of such galaxies in the field is practically close to the fraction for clusters only among the most massive systems (Fig. 5e), especially in the massive system A 1656. The are few galaxies in this interval in less massive systems.

Galaxies with ongoing and suppressed star formation have different velocity radial-velocity dispersions, which in the former are 10–35% higher than in the latter [4]. To demonstrate this, we show the dependence of the space distribution of galaxies and their kinematic properties on specific star-formation rate subdivided into four bins (Fig. 6). The sizes of symbols in the figure correspond to these bins: the large symbols correspond to "active" galaxies with $\log sSFR[\mathrm{Gyr}^{-1}] = -1.75 \ldots -1.35$, $-1.35 \ldots -1.05$; the small symbols, to galaxies with suppressed star formation with $\log sSFR[\mathrm{Gyr}^{-1}] = -1.75 \ldots -4.00$, and -4.00—all the remaining galaxies. For each bin we determined the average clustercentric distance of population members normalized to the cluster radius $R_{200\mathrm{c}}$, $\langle R \rangle / R_{200\mathrm{c}}$, and the dispersion of their radial velocities normalized to the radial-velocity dispersion of the cluster within $R_{200\mathrm{c}}$. The large symbols denote "active" galaxies with ongoing star formation and small symbols, galaxies with suppressed star formation. All galaxy clusters exhibit a common trend—galaxies with ongoing star formation (especially those with $\log sSFR > -1.35$) are, as a population, located far from the cluster center and have higher radial-velocity dispersions than galaxies with suppressed star formation. These objects, which are located outside the virial radius $R_{200\mathrm{c}}$, most likely form the population of infall galaxies—the future members of of the cluster.

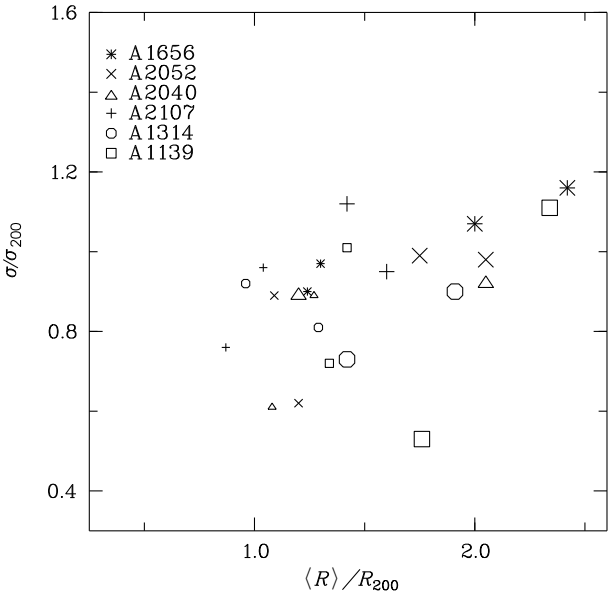

Fig. 6. Variation of the space distribution and kinematics of galaxies in clusters as a function of their specific star-formation rate ($\log sSFR$) in four bins. The bins $\log sSFR[\mathrm{Gyr}^{-1}] = -1.75 \ldots -1.35, -1.35 \ldots -1.05$ and, correspondingly, "active" galaxies where stars firm are indicated by large symbol, whereas small symbols indicate the bins $\log sSFR[\mathrm{Gyr}^{-1}] = -1.75 \ldots -4.00$, -4.00—the remaining objects (galaxies with suppressed star formation).

Table 2 presents the results of the measurements of the fraction of quenched galaxies along the normalized cluster radius and the fraction of early-type galaxies on the RS. Column (1) gives the name of the system, and the other columns give the range of normalized radii ($R/R_{200\mathrm{c}}$ and R_{sp}). The first line gives the fraction of early-type galaxies on the RS, $frac_E$, and the second column, the fraction of galaxies with suppressed star formation, $frac_q$.

Table 2. Variation of the fraction of early-type galaxies and galaxies with suppressed star formation along the radius

Cluster	Fraction	$0{-}0.25\,R/R_{200c}$	$0{-}1\,R/R_{200c}$	$1{-}2\,R/R_{200c}$	$2{-}3\,R/R_{200c}$	$0{-}1\,R_{sp}$	$1R_{sp}{-}3R/R_{200c}$
A 1656	$frac_E$	0.73 ± 0.11	0.54 ± 0.05	0.50 ± 0.07	0.25 ± 0.06	0.50 ± 0.04	0.22 ± 0.03
	$frac_q$	0.79 ± 0.12	0.75 ± 0.06	0.68 ± 0.09	0.42 ± 0.09	0.74 ± 0.05	0.42 ± 0.08
A 1314	$frac_E$	0.57 ± 0.25	0.51 ± 0.12	0.50 ± 0.23	0.33 ± 0.22	0.51 ± 0.11	0.36 ± 0.16
	$frac_q$	0.93 ± 0.36	0.77 ± 0.16	0.57 ± 0.25	0.33 ± 0.22	0.74 ± 0.14	0.36 ± 0.21
A 2052	$frac_E$	0.50 ± 0.18	0.52 ± 0.10	0.36 ± 0.11	0.26 ± 0.06	0.49 ± 0.09	0.23 ± 0.05
	$frac_q$	0.91 ± 0.28	0.84 ± 0.14	0.45 ± 0.12	0.42 ± 0.09	0.80 ± 0.13	0.41 ± 0.08
A 1139	$frac_E$	0.62 ± 0.35	0.44 ± 0.10	0.15 ± 0.08	0.15 ± 0.12	0.36 ± 0.08	0.20 ± 0.07
	$frac_q$	0.86 ± 0.34	0.64 ± 0.12	0.27 ± 0.12	0.45 ± 0.15	0.64 ± 0.12	0.37 ± 0.10
A 2107	$frac_E$	0.69 ± 0.19	0.57 ± 0.06	0.38 ± 0.09	0.28 ± 0.10	0.50 ± 0.08	0.31 ± 0.08
	$frac_q$	0.91 ± 0.23	0.78 ± 0.12	0.56 ± 0.13	0.55 ± 0.17	0.73 ± 0.10	0.55 ± 0.15
A 2040	$frac_E$	0.64 ± 0.20	0.49 ± 0.09	0.27 ± 0.08	0.22 ± 0.08	0.43 ± 0.07	0.20 ± 0.05
	$frac_q$	0.84 ± 0.25	0.67 ± 0.11	0.51 ± 0.12	0.40 ± 0.12	0.61 ± 0.09	0.45 ± 0.11

5. CONCLUSIONS

In the field (outside clusters and groups of galaxies) the morphology of galaxies and star formation in them are independent of each other—low star formation rate is associated with early-type galaxies, whereas high star formation rate is found in late-type, spiral galaxies. Galaxies in clusters come under special conditions, they are more affected by hot virialized gas inside clusters, whereas other galaxies exert less influence. Furthermore, galaxies falling into clusters together with groups are supposed to have already been affected by the gas of the groups (see, e.g., [4]). Simulations demonstrate radial gradient of star formation in galaxy clusters, which reflects the dependence of galaxy properties on the clustercentric distance and time when they accreted onto the cluster (see, e.g., [3]). The phase-space diagrams that relate the projected radial-velocity dispersions and projected clustercentric distance, are most suitable for studying this phenomenon (see, e.g., [4, 9–11, 14]).

We used SDSS catalog data for six galaxy clusters, A 1656, A 1139, A 1314, A 2040, A 2052, and A 2107, to investigate the gradients of specific star formation rate along the radius, determined the fraction of galaxies with suppressed star formation within the virialized regions and in within the nearest outskirt (out to $3R/R_{200c}$) and compared the results with those for field galaxies.

We obtained the following results:

(1) The specific star formation rate in the galaxy systems studied ($\log M_{200c}[M_\odot] = 14.21{-}15.12$) has a peak at $\log sSFR[\mathrm{Gyr}^{-1}] \approx -2.2$, and the adopted minimum in the distribution is at the value of $\log sSFR[\mathrm{Gyr}^{-1}] \approx -1.75$, which we use to separate objects into "active" galaxies with ongoing star formation and galaxies with suppressed star formation.

(2) Galaxy clusters show radial gradient of $sSFR$. The fraction of galaxies with suppressed star formation is maximal in central regions amounting to 0.87 ± 0.02 within $2{-}3\,R/R_{200c}$, whereas it is equal to 0.43 ± 0.03 beyond R_{sp}. This value that we obtained for peripheries of galaxy clusters is greater by 26% than the corresponding value for field galaxies. Significant variations of the fraction of galaxies with suppressed star formation along the radius are observed in systems with stellar masses $\log M_\star[M_\odot] = 9.5{-}10.0$ (the only exception is the cluster A 1656 with $M_{200c}[M_\odot] > 10^{15}$). Galaxies with ongoing star formation in clusters have, on the average, higher radial-velocity dispersions and are located farther from the center.

(3) The red sequence of early-type galaxies with a small scatter is the main feature of galaxy clusters, because their virialized regions consist of luminous early-type galaxies, which make up for 60–70% of such objects. We show that outside R_{sp} the fraction of $frac_E$ (within $2{-}3\,R/R_{200c}$) becomes as low as in the field.

ACKNOWLEDGMENTS

This research has made use of the NASA/IPAC Extragalactic Database (NED, http://nedwww.ipac.caltech.edu), which is operated by the Jet Propulsion Laboratory, California Institute of Technology, under contract with the National Aeronautics and Space Administration, Sloan Digital Sky Survey (SDSS, http://www.sdss.org), which is supported by Alfred P. Sloan Foundation, the participant institutes of the SDSS collaboration, National Science Foundation, and the United States Department of Energy and Two Micron All Sky Survey (2MASS, http://www.ipac.caltech.edu/2mass/releases/allsky/).

REFERENCES

1. A. Boselli and G. Gavazzi, Publ. Astron. Soc. Pacific **118**, 517 (2006).
2. M. L. Balogh, S. L.Morris, H. K. C. Yee, et al., Astrophys. J. **527**, 54 (1999).
3. M. L. Balogh, J. F. Navarro, and S. L. Morris, Astrophys. J. **540**, 113 (2000).
4. C. P. Haines, M. J. Pereira, G. P. Smith, et al., Astrophys. J. **775**, 126 (2013).
5. A. R. Wetzel, J. L. Tinker, and C. Conroy, Monthly Notices Royal Astron. Soc. **424**, 232 (2012).
6. S. P. D. Gill, A. Knebe, and B. K. Gibson, Monthly Notices Royal Astron. Soc. **356**, 1327 (2005).
7. E. Zinger, A. Dekel, A. V. Kravtsov, and D. Nagai, arXiv:1610.02644 (2016).
8. A. Paccagnella, B. Vulcani, B. M. Poggianti, et al., Astrophys. J.**816**, L25 (2016).
9. S. Mahajan, G. A. Mamon, and S. Raychaudhury, Monthly Notices Royal Astron. Soc. **418**, 2816 (2011).
10. J. D. Hernández-Fernández, C. P. Haines, A. Diaferio, et al., Monthly Notices Royal Astron. Soc. **438**, 2186 (2014).
11. A. Muzzin, R. F. J. van der Burg, S. L. McGee, et al., Astrophys. J. **796**, 65 (2014).
12. K. A. Oman, M. J. Hudson, and P. S. Behroozi, Monthly Notices Royal Astron. Soc. **431**, 2307 (2013).
13. K. A. Oman and M. J. Hudson, Monthly Notices Royal Astron. Soc. **463**, 3083 (2016).
14. J. Rhee, R. Smith, H. Choi, et al., Astrophys. J. **843**, 128 (2017).
15. S. Alam, F. D. Albareti, C. Allende Prieto, et al., Astrophys. J. Suppl. **219**, 12 (2015).
16. T. H. Jarrett, T. Chester, R. Cutri, et al., Astron. J. **119**, 2498 (2000).
17. M. A. Strauss, D. H. Weinberg, R. H. Lupton, et al., Astron. J. **124**, 1810 (2002).
18. A. Sandage, Astrophys. J. **176**, 21 (1972).
19. F. G. Kopylova, Astrophysical Bulletin **68**, 253 (2013).
20. R. G. Carlberg, H. K. C. Yee, and E. Ellingson, Astrophys. J. **478**, 462 (1997).
21. V. R. Eke, S. Cole, and C. S. Frenk, Monthly Notices Royal Astron. Soc. **282** (1996).
22. F. G. Kopylova and A. I. Kopylov, Astronomy Letters **37**, 219 (2011).
23. F. G. Kopylova and A. I. Kopylov, Astronomy Letters **39**, 1 (2013).
24. A. I. Kopylov and F. G. Kopylova, Astrophysical Bulletin **70**, 243 (2015).
25. G. A. Mamon, T. Sanchis, E. Salvador-Solé, and J. M. Solanes, Astron. and Astrophys. **414**, 445 (2004).
26. S. More, B. Diemer, and A. V. Kravtsov, Astrophys. J. **810**, 36 (2015).
27. R. B. Tully, Astron. J. **149**, 54 (2015).
28. S. More, H. Miyatake, M. Takada, et al., Astrophys. J. **825**, 39 (2016).
29. C. Chang, E. Baxter, B. Jain, et al., arXiv:1710.06808 (2017).
30. A. Dressler, Annual Rev. Astron. Astrophys. **22**, 185 (1984).
31. O. López-Cruz, W. A. Barkhouse, and H. K. C. Yee, Astrophys. J. **614**, 679 (2004).
32. N. Visvanathan and A. Sandage, Astrophys. J. **216**, 214 (1977).
33. B. M. Tinsley, Astrophys. J. **151**, 547 (1968).
34. R. B. Larson, B. M. Tinsley, and C. N. Caldwell, Astrophys. J. **237**, 692 (1980).
35. C. Conroy, J. E. Gunn, and M. White, Astrophys. J. **699**, 486 (2009).
36. A. R. Wetzel, J. L. Tinker, C. Conroy, and F. C. van den Bosch, Monthly Notices Royal Astron. Soc. **439**, 2687 (2014).
37. S. P. Bamford, R. C. Nichol, I. K. Baldry, et al., Monthly Notices Royal Astron. Soc. **393**, 1324 (2009).

Translated by A. Dambis